Eur. Phys. J. Plus (2018) **133**: 225
DOI 10.1140/epjp/i2018-12056-4

THE EUROPEAN PHYSICAL JOURNAL PLUS

Regular Article

Probing the geometries and electronic properties of iridium-doped silicon Ir_2Si_n (n = 1–18) clusters*

Tie Ye[1], Ming Hui[2,a], Yu Zhang[1], Ai-Hua Wang[2,b], Zhuo Wang[1], and Gen-Quan Li[1]

[1] Mechanical and electronic engineering institute, Nanyang Normal University, Nanyang 473061, China
[2] Physics and electronic engineering institute, Nanyang Normal University, Nanyang 473061, China

Received: 4 December 2017 / Revised: 18 April 2018
Published online: 14 June 2018

Abstract. The effect of double Ir atoms doping on the geometries and electronic properties of silicon clusters has been studied in detail using the density functional theory at B3LYP level. Compared with silicon clusters, the geometric structures of the ground state Ir_2Si_n clusters show different appearance except for Ir_2Si_8. The analysis of stability revealed that Ir_2Si_6, Ir_2Si_9 and Ir_2Si_{11} have more stable features in all studied clusters and the doping of Ir atoms makes the stabilities of Si_n clusters decrease. The analysis of internal charge transfer shows that the Ir atoms always possess negative charge and strong spd hybridization exists in the Ir atoms. The results of electrostatic potential indicates that a negative potential surrounds Ir atoms. Finally, the infrared and Raman spectrums of $Ir_2Si_{6,9,11}$ clusters are discussed.

1 Introduction

As an effective bridge between bulk materials and atomic or molecular structures, clusters have attracted great attention so far [1–6]. The investigations of these nano-scale clusters are expected to design and synthesize some novel functional materials with special properties. In recent years, much of the interest in silicon and doped silicon clusters has been fuelled by their novel applications in the fields of microelectronics, catalysis, surface film, data storage, power source and optical materials. In particular, since transition metal (TM) atoms have an unfilled d orbital, their electronic characteristics hinge on the interaction between s and d electrons and can dramatically impact the electronic structure of a pure Si_n cluster [7–9]. Therefore, the TM atoms doped in the Si_n clusters have become an important topic for experimental and theoretical investigations on their geometrical structures and electronic properties [10–15]. Koyasu *et al.* [10] examined the structural and electronic properties of Si_nX (X = Y, Ti, Sc, Nb, Lu, Zr, Ta, V and Hf) clusters using mass spectrometry and anion photoelectron spectra (PES). Ngan *et al.* [11] observed the spectra of Mn-doped silicon Si_nMn^+ clusters using mass spectrometry. Lievens *et al.* [12] investigated the geometries of $CoSi_n$ (n = 10–12) clusters using the infrared-ultraviolet two-color ionization (IR-UV2CI) method in combination with theoretical calculations. Their results indicated that the $CoSi_n$ clusters have endohedral caged structures. Theoretical work by Robles and Khanna [13,14] demonstrated that the T_2Si_n (T = Cr, Mn, Fe, Co, Ni, n = 1–8) clusters display a variety of magnetic species with varying magnetic moment and different magnetic coupling between the two transition metal atoms. Bandyopadhyay [15] explored the geometric structures of MSi_n (M = Ti, Zr, Hf; n = 9–20) and found that Si_{16}(a)M is always magic under neutral condition. Nakajima *et al.* [16] studied the geometric, electronic, and optical properties of M@Si_{16} (M = Sc, Ti, V) clusters with D_{4d} symmetry and found that Sc@Si_{16}-V@Si_{16} and Sc@Si_{16}-Ti@Si_{16}-V@Si_{16} show large HOMO-LUMO gaps (2.8 and 2.4 eV). Lu *et al.* [17] made a theoretical study on the geometries, charge population, and polarizability of Pd_2Si_n (n = 1–12) clusters, and they found that one Pd atom starts to fall into the internal location of the Si_n cage from n = 10. Based on the crystal structure analysis by particle swarm optimization (CALYPSO) geometry searching program, Kuang *et al.* [18] studied the ground state $NbSi_n{}^Q$ (n = 2–20;

* Supplementary material in the form of a .pdf file available from the Journal web page at https://doi.org/10.1140/epjp/i2018-12056-4

[a] e-mail: huimingsn@163.com
[b] e-mail: nynuaihuawang@163.com (corresponding author)

Table 1. Comparison of our calculated bond length r (Å), frequency ω (cm^{-1}), binding energies E (eV), vertical ionization potential VIP (eV) and dissociation energies D (eV) with experimental (Exp.) results.

Method	IrSi			Ir_2			Si_2		
	r	ω	E	r	ω	D	r	ω	VIP
PW91	2.12	532.90	6.04	2.26	280.89	5.33	2.30	468.7	8.25
PBE	2.12	532.05	6.01	2.26	280.51	5.31	2.30	468.8	8.21
BP86	2.12	530.36	6.00	2.26	280.10	5.19	2.30	465.6	8.30
B3LYP	2.11	536.15	4.73	2.26	284.38	3.27	2.28	485.5	8.60
Exp.	$2.09^{(a)}$	$533^{(a)}$	$4.76 \pm 0.22^{(a)}$	$2.35^{(b)}$	$280^{(b)}$	$3.46 \pm 0.12^{(c)}$	$2.25^{(d)}$	$511.0^{(d)}$	$> 8.49^{(e)}$

(a) Ref. [38]. (b) Ref. [39]. (c) Ref. [40]. (d) Ref. [41]. (e) Ref. [42].

$Q = 0, \pm 1$) clusters and found that the Nb atom moves gradually from the surface site to the encapsulated site with cluster size growing. Recently, Zhang *et al.* [19] studied the electronic properties of neutral and charged $Rh_2Si_n{}^{0,\pm1}$ (n = 1–10) clusters. Their results showed that the $Rh_2Si_6{}^{0,\pm1}$ clusters have more stabilities than the other ones.

The TM Ir atom is an active component of organic catalysts, which plays an important role in catalysis. In particular, iridium silicide has attracted more and more attention, both in experiment and theory [20–22], because of its potential applications in the fields of infrared detection in Schottky barrier devices, cold cathode field emission display, and so on. Despite enormous investigations of TM-atoms–doped silicon clusters have been reported, relatively few theoretical studies are available on the one-iridium–doped Si_n clusters. The formation of small $IrSi_n^+$ and $IrSi_nH_{2n}^+$ clusters was first reported by Hiura and coworkers [23] using an ion trap. The major finding of this study shows that the $IrSi_2^+$ cluster has relative abundance compared to other clusters. Han [24] studied the structures, charge population, and magnetism of Si_nIr (n = 1–6) clusters and found that the charge transfer from Si atoms to Ir atom is sensitively associated with spin multiplicity. So far, no theoretical reports are available on the structural evolution and electronic properties of Si_n clusters with iridium molecule. Two questions arise: 1) With what size of Si_n cluster will the Ir atoms form an Ir-encapsulted Si cage? 2) Are there obvious differences between silicon clusters with one Ir doping and silicon clusters with double Ir atoms? To obtain more detailed information on Ir_2Si_n clusters, it is necessary to study the evolution of cluster properties with the size of the system.

2 Computational methods

To find the most stable Ir_2Si_n (n = 1–18) clusters, a large amount of initial geometries is considered in the following ways: i) many previous studies on the pure Si_n [25–28] and TM_2Si_n [29–34] clusters are employed as a guide; ii) placing or capping Ir atoms at various sites of Si_n clusters as well as substituting two TM atoms of TM_2Si_n clusters by the Ir atoms. By use of the above methods, many optimized isomers for the Ir_2Si_n cluster are obtained. The calculations are performed using the spin-unrestricted DFT method with the hybrid B3LYP function [35, 36]. The effective core potential LANL2DZ basis set for TM Ir atom and full electron 6-311+G(d) basis set for Si atom is chosen. The effects of the spin polarization have been taken into account (singlet, triplet, quintet and septet) and no symmetry constraints are performed in the geometry optimization. All calculations are performed using the Gaussian 09 program [37]. Due to the lack of experimental data, it is difficult to say that the obtained isomers are the ground state structures. But since the size of Ir_2Si_n clusters is small, leading the amount of isomers for each cluster size is rather limited. So, we can identify the optimized structures corresponding to a local minimum.

To ensure the reliability of the whole system, we first carry out calculations on the IrSi, Si_2 and Ir_2 dimers with different theoretical methods (PW91, PBE, BP86, and B3LYP) with the GENECP basis set. The results with the experimental value [38–42] are summarized in table 1. From the data listed in table 1, it can be seen that the calculated results of r (bond length), ω (frequency), E (binding energies), VIP (vertical ionization potential) and D (dissociation energies) at B3LYP level are in accordance with the experimental data. Therefore, the B3LYP functional is adopted in the current study.

3 Results and discussions

3.1 Structures

The most stable and some metastable isomers of Ir_2Si_n (n = 1–18) clusters are depicted in figs. 1–3. The symmetry, electronic state and relative energy is given below the isomer. Besides, the geometries of most stable Si_{n+2} clusters are also illustrated in the Supplementary Material (fig. S1) for comparison, which is consistent with previous articles [21–24]. The calculated Ir-Ir bond lengths, and total energies are listed in table 2. The bond lengths in cage-like Ir_2Si_{15-18} clusters are plotted in fig. S2.

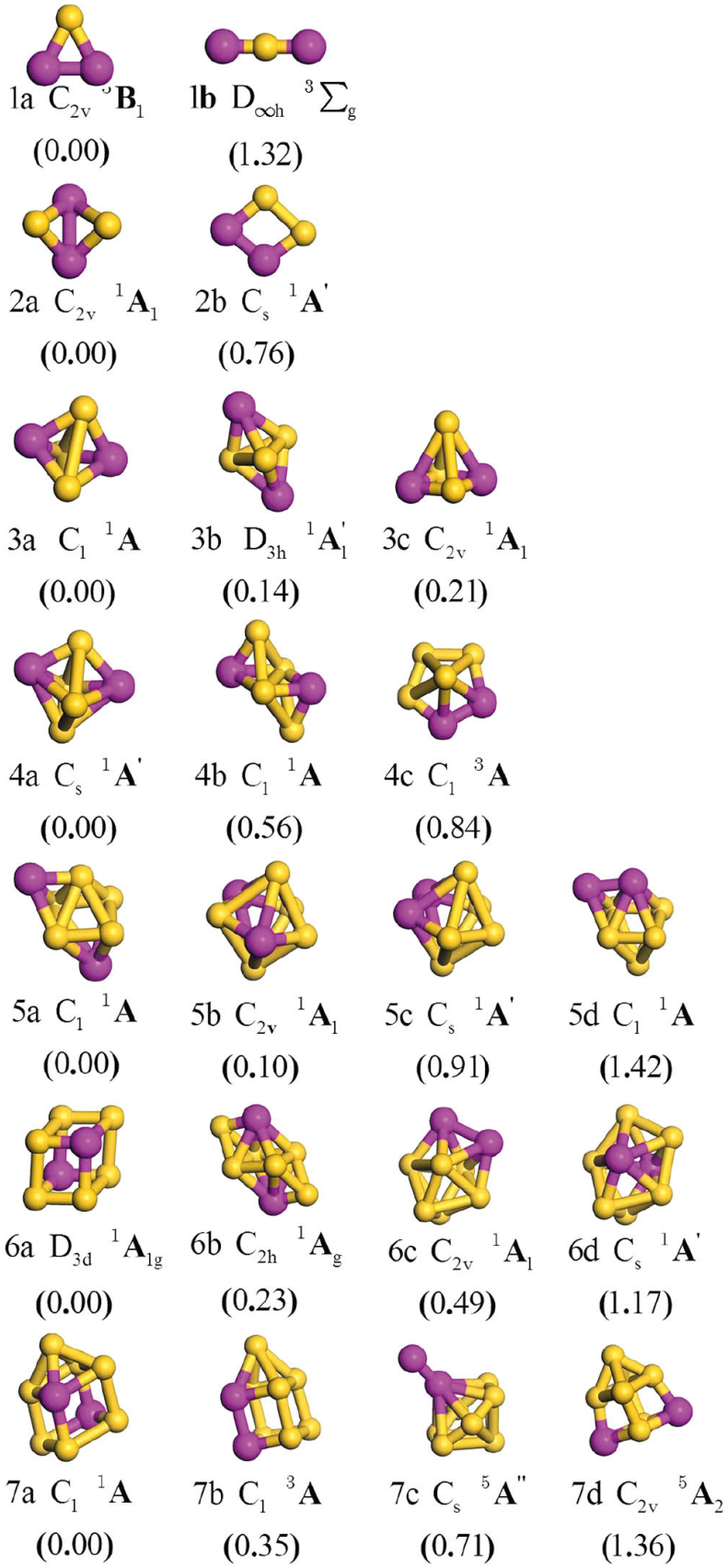

Fig. 1. The lowest-energy structures of Ir_2Si_n (n = 1–7), and a few low-lying isomers for doped clusters. Yellow and purple balls represent Si and Ir atoms, respectively.

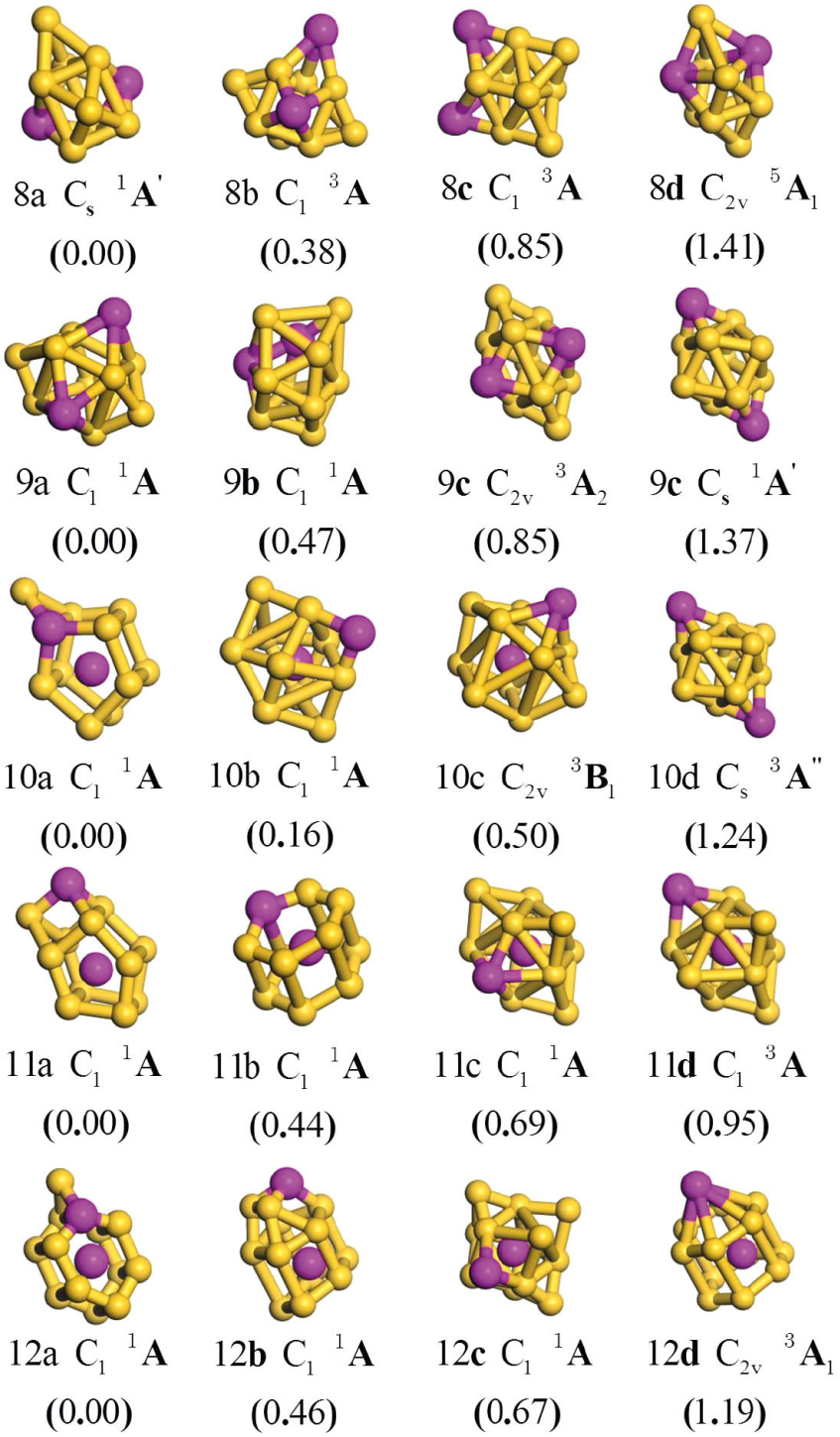

Fig. 2. The lowest-energy structures of Ir_2Si_n (n = 8–12), and a few low-lying isomers for doped clusters. Yellow and purple balls represent Si and Ir atoms, respectively.

For Ir_2Si cluster, the most stable isomer (1a) is an isosceles triangle with C_{2v} symmetry and its Ir-Si-Ir apex angle is 62.72°, in which two Ir atoms locate at two sides. The isomer 1b is a linear structure with $D_{\infty h}$ symmetry. At $n = 2$, the ground state 2a isomer with C_{2v} symmetry has a butterfly structure, which resembles the structures of lowest-energy Cu_2Si_2, Pd_2Si_2, and Rh_2Si_2 [29,30,33] clusters. The rhombus 2b isomer resembles the structure of ground state Si_4 (fig. S1). Among Ir_2Si_3 cluster, the boat isomer 3a is found to be the most stable structure. The 3b isomer is a trigonal bipyramid structure. The pyramid 3c isomer resembles the structure of lowest-energy Si_5 (fig. S1). When $n = 4$, the most stable structure (4a) can be seen as a Si atom capping on the top of the 3a isomer, forming a

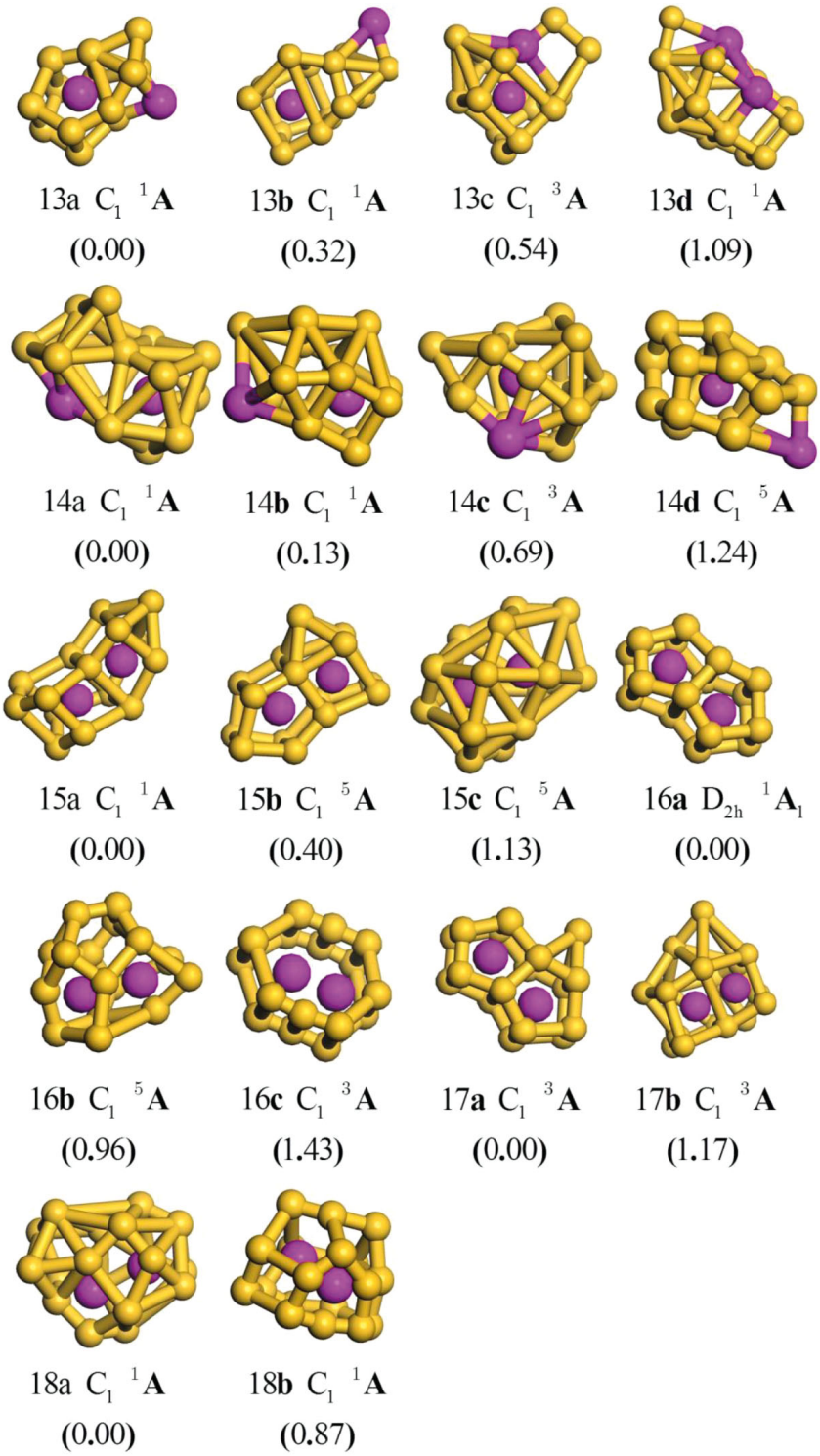

Fig. 3. The lowest-energy structures of Ir_2Si_n (n = 13–18), and a few low-lying isomers for doped clusters. Yellow and purple balls represent Si and Ir atoms, respectively.

face capped tetragonal bipyramid. The 3D 4b isomer coincides with that for Zr_2Si_4 obtained by Zhang *et al.* [33]. The 4c isomer has a pentagonal pyramid structure. For $n = 5$, the ground state Ir_2Si_5 (5a) cluster is generated by capping the tetragonal dipyramid structure with an Ir atom. Similar to the structure of the most stable Si_7 cluster (fig. S1), the isomers 5b and 5c can be regarded as two substituted structures, in which two Ir atoms replace different Si atoms of a pentagonal bipyramid Si_7. The 5d isomer shows a similar geometry to the low-lying isomer of Pd_2Si_5 [30]. For $n = 6$, the optimized results reveal that the hexahedron-structure 6a one is the most stable isomer. The 6b isomer can

Table 2. The calculated Ir-Ir bond lengths Ir-Ir (Å), total energies E_T (a.u.), averaged binding energy E_b (eV), dissociation energy E_f (eV), second-order energy difference $\Delta_2 E$ (eV), and HOMO-LUMO energy gaps $E_{\rm gap}$ of the lowest-energy Ir_2Si_n ($n = 1$–18) clusters.

n	Ir-Ir	E_T	E_b	E_f	$\Delta_2 E$	$E_{\rm gap}$
1	2.38	−498.85	2.43			2.58
2	2.57	−788.44	2.97	6.34	0.41	2.15
3	3.25	−1078.01	3.13	5.93	2.71	2.32
4	3.24	−1367.47	3.25	3.22	−2.27	1.79
5	3.56	−1657.03	3.40	5.49	−0.12	1.67
6	3.26	−1946.59	3.30	5.62	1.80	1.87
7	2.96	−2236.08	3.43	3.82	−0.29	1.74
8	2.80	−2525.58	3.37	4.11	−1.13	1.69
9	3.32	−2815.13	3.43	5.24	0.32	1.76
10	2.72	−3104.66	3.45	4.92	−0.43	1.69
11	3.54	−3394.21	3.51	5.35	0.47	1.40
12	2.88	−3683.74	3.53	4.88	0.62	1.99
13	3.74	−3973.25	3.54	4.26	0.30	1.50
14	2.84	−4262.74	3.50	3.98	−1.13	1.87
15	2.91	−4552.28	3.52	5.12	−1.47	1.76
16	2.58	−4841.88	3.63	6.59	2.64	1.84
17	2.69	−5131.38	3.59	3.94	1.76	1.55
18	3.04	−5420.81	3.46	2.18		1.38

be seen as two Si atoms in the most stable Si_8 (fig. S1) cluster are substituted by Ir atoms. The 6c and 6d isomers have a similar geometry in which the Ir atoms occupy different places. On the basis of the 6a isomer, two derived structures (7a and 7b) are generated by capping the 6a isomer with one Si atom. The former is more stable than the latter. The 7c isomer can be seen as one Ir atom capping on the apex position of a hexagonal bipyramid structure. The 7d isomer is generated when two Si atoms in the most stable Si_9 cluster (fig. S1) are replaced by Ir atoms.

Compared to the corresponding Si_{10} (fig. S1) cluster, the 8a and 8b isomers can be seen as two substituting structures of Si_{10} clusters. The latter is 0.38 eV higher in energy than that of former. The 8c isomer is a derived geometry of the 6b isomer after two Ir atoms are capped on it. The 8d isomer resembles the most stable geometry of Rh_2Si_8 [33]. With regard to Ir_2Si_9 cluster, the most stable 9a isomer possesses a 3D geometry, which is obtained by capping a Si atom on the triangular face of the 8a isomer. When a Si atom is capped on the tetragonal face of the 8d isomer, the 9b isomer is generated. The 9c and 9d isomers can be generated by replacing different Si atoms in the structure of most stable Si_{11} (fig. S1). As for Ir_2Si_{10} cluster, the 10a isomer, which is obtained after a Si atom is capped on the Ir-centered pentagonal prism Si_{10} structure, is found to be most stable geometry. It is worth noting that the isomer 10a is the first structure in which one Ir atom is encapsulated into the Si_n frame. After the free Ir_2 dimer is inserted into the Si_{10} frame, the Ir-Ir bond length (2.72 Å) in the Ir_2Si_{10} cluster is apparently elongated. The 10b isomer is a cubic geometry in which one Ir atom being surface capped on the $IrSi_9$ frame after another Ir atom being encapsulated into the Si_9 cage. When one Ir atom occupies the interior site of 9a, the derived 10c isomer is generated. The 10d isomer is a substituted structure in which two Ir atoms replace the Si atoms of Si_{11} (fig. S1). For $n = 11$, the most stable 11a isomer is optimized by capping the ground state Ir_2Si_{10} cluster with one Si atom. The Ir-Ir bond length is 3.54 Å. The 11b isomer has an Ir-centered hexagonal prism structure. Two other 3D low-lying isomers (11c and 11d) can be seen as a derived version of the 10d isomer. With respect to the cluster Ir_2Si_{12}, the calculated results shown that the stereoscopic 12a isomer is the most stable geometry with Ir-Ir bond length of 2.88 Å. The 12b isomer is generated when a Si atom is added to the 11a isomer. The 12c isomer is considered to be a derived structure of the 11c isomer. The 12d isomer shows a similar geometry to the metastable isomer of Mo_2Si_{12} [30]. At $n = 13$, the 13a structure is generated after one Si atom is surface capped on the pentagonal prism-like isomer 12a. For Ir_2Si_{14}, the isomer 14a, which is generated after one Si atom is surface capped on the isomer 13c, is optimized to be the most stable isomer. As n is in the range from 15 to 18, the clusters contain two Ir atoms with the other Si atoms forming a cage.

From the above discussions, one can easily find that the structures of the most stable Ir_2Si_n clusters favor the 3D geometries from $n = 2$. Most of them have a different structure from the corresponding Si_{n+2} clusters with the exception of Ir_2Si_8, implying that the doping of Ir atoms obviously effect the framework of Si_{n+2} clusters. One Ir atom prefers to occupy the interior site of the Si_n cluster in the range of $n = 10$–14, which is in accordance with the previous reports about $TM_2@Si_n$ (TM = Pd and Mo) [30,32] clusters. Starting from $n = 15$, two Ir atoms completely fall into the inner of the Si_n cage.

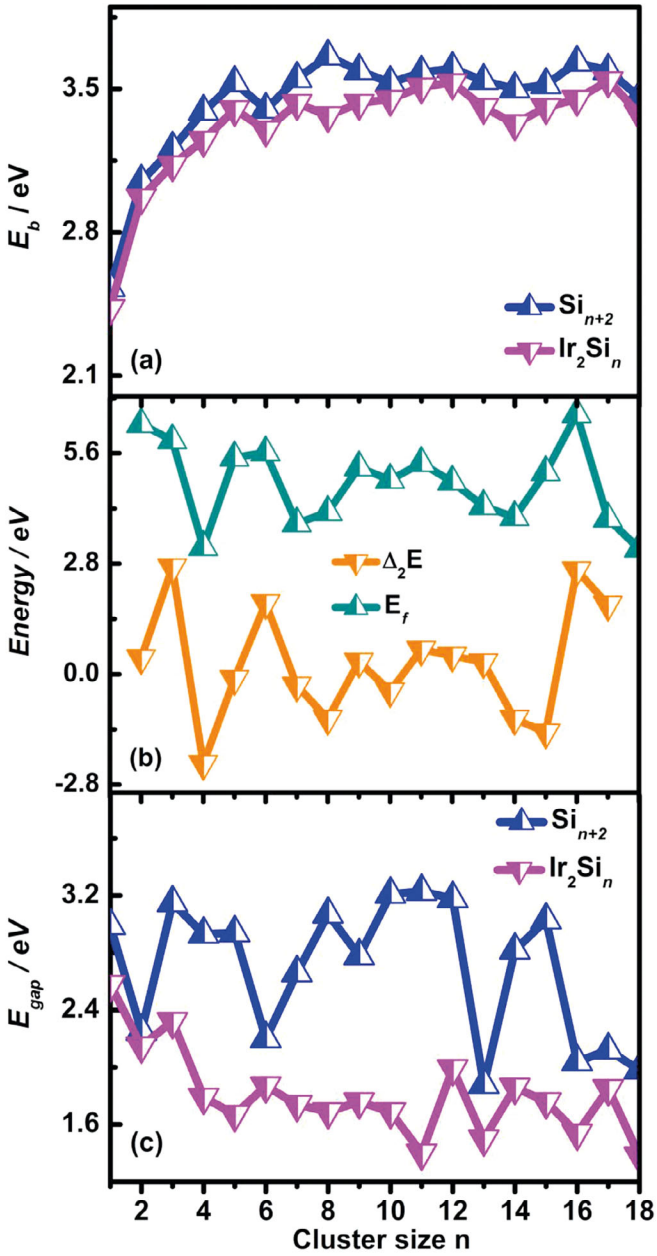

Fig. 4. The size dependence of the averaged binding energy E_b (a), dissociation energy E_f (b), second-order difference energy $\Delta_2 E$ (b), and HOMO-LUMO energy gap $E_{\rm gap}$ (c) of the most stable Ir_2Si_n ($n = 1$–18) clusters.

3.2 Relative stabilities

Table 2 provides the energetic characteristics of ground state Ir_2Si_n ($n = 1$–18) clusters. In general, the average binding energy (E_b), dissociation energy (E_f), second-order energy difference ($\Delta_2 E$), and HOMO-LUMO energy gaps ($E_{\rm gap}$) of a given cluster are sensitive qualities of its relative stabilities. For Ir_2Si_n clusters, the E_b, E_f, and $\Delta_2 E$ are defined as follows:

$$E_b(\mathrm{Ir_2Si}_n) = [nE_t(\mathrm{Si}) + 2E_t(\mathrm{Ir}) - E_t(\mathrm{Ir_2Si}_n)]/(n+2), \quad (1)$$

$$E_f(\mathrm{Ir_2Si}_n) = E_t(\mathrm{Ir_2Si}_{n-1}) + E_t(\mathrm{Si}) - E_t(\mathrm{Ir_2Si}_n), \quad (2)$$

$$\Delta_2 E(\mathrm{Ir_2Si}_n) = E_t(\mathrm{Ir_2Si}_{n+1}) + E_t(\mathrm{Ir_2Si}_{n-1}) - 2E_t(\mathrm{Ir_2Si}_n). \quad (3)$$

The results of corresponding characteristics are depicted in figs. 4(a), (b) and (c) and summarized in table 2. To compare the results, the $E_b(n)$ and $E_{\rm gap}$ of corresponding Si_{n+2} clusters are also computed and plotted in figs. 4(a) and (c).

Table 3. Natural electronic configuration (NEC) of Ir and Si atoms in the ground state Ir_2Si_n (n = 1–18) clusters, natural population analysis (NPA) of Ir atoms in the most stable Ir_2Si_n clusters, where Ir-1 and Ir-2 correspond to the left (or top) and right (or bottom) Ir atoms in figs. 1–3.

n	NEC			NPA	
	Ir-1	Ir-1	Si	Ir-1	Ir-1
1	$6s^{0.94}5d^{8.16}6p^{0.10}$	$6s^{0.94}5d^{8.16}6p^{0.10}$	$3s^{1.80}3p^{1.76}$	−0.20	−0.20
2	$6s^{0.75}5d^{8.56}6p^{0.21}$	$6s^{0.75}5d^{8.56}6p^{0.21}$	$3s^{1.72}3p^{1.73}$	−0.52	−0.52
3	$6s^{0.81}5d^{8.74}6p^{0.26}$	$6s^{0.81}5d^{8.74}6p^{0.26}$	$3s^{1.68}3p^{1.73}$	−0.82	−0.82
4	$6s^{0.70}5d^{8.72}6p^{0.27}$	$6s^{0.69}5d^{8.74}6p^{0.25}$	$3s^{1.61-1.66}3p^{1.70-2.18}$	−0.70	−0.69
5	$6s^{0.74}5d^{8.77}6p^{0.41}$	$6s^{0.72}5d^{8.73}6p^{0.48}$	$3s^{1.53-1.66}3p^{1.81-2.24}$	−0.91	−0.94
6	$6s^{0.66}5d^{8.72}6p^{0.48}$	$6s^{0.66}5d^{8.72}6p^{0.48}$	$3s^{1.56}3p^{2.11}$	−0.86	−0.86
7	$6s^{0.66}5d^{8.92}6p^{1.45}$	$6s^{0.60}5d^{8.71}6p^{0.35}$	$3s^{1.43-1.69}3p^{2.23-2.95}$	−2.04	−0.67
8	$6s^{0.68}5d^{8.92}6p^{1.36}$	$6s^{0.58}5d^{8.70}6p^{0.31}$	$3s^{1.43-1.69}3p^{2.23-2.95}$	−1.97	−0.59
9	$6s^{1.71}5d^{9.00}6p^{1.50}$	$6s^{0.61}5d^{8.80}6p^{0.34}$	$3s^{1.35-1.71}3p^{1.59-2.27}$	−2.17	−0.76
10	$6s^{0.56}5d^{9.20}6p^{2.13}$	$6s^{0.58}5d^{8.69}6p^{0.57}$	$3s^{1.38-1.67}3p^{1.71-2.48}$	−2.91	−0.64
11	$6s^{0.56}5d^{9.18}6p^{2.26}$	$6s^{0.58}5d^{8.72}6p^{0.15}$	$3s^{1.28-1.62}3p^{1.97-2.27}$	−3.04	−0.45
12	$6s^{0.53}5d^{8.99}6p^{1.65}$	$6s^{0.59}5d^{8.74}6p^{0.50}$	$3s^{1.28-1.62}3p^{1.97-2.27}$	−2.20	−0.81
13	$6s^{0.57}5d^{9.08}6p^{1.95}$	$6s^{0.58}5d^{8.79}6p^{0.18}$	$3s^{1.32-1.55}3p^{2.13-2.52}$	−2.62	−0.55
14	$6s^{0.60}5d^{9.02}6p^{1.75}$	$6s^{0.59}5d^{9.03}6p^{1.66}$	$3s^{1.32-1.67}3p^{1.76-2.49}$	−2.48	−1.99
15	$6s^{0.56}5d^{9.14}6p^{1.85}$	$6s^{0.59}5d^{9.05}6p^{1.62}$	$3s^{1.28-1.60}3p^{1.88-2.45}$	−2.56	−2.28
16	$6s^{0.50}5d^{9.01}6p^{1.76}$	$6s^{0.50}5d^{9.01}6p^{1.76}$	$3s^{1.30-1.562}3p^{2.13-2.41}$	−2.29	−2.29
17	$6s^{0.51}5d^{9.01}6p^{1.74}$	$6s^{0.50}5d^{9.08}6p^{1.74}$	$3s^{1.29-1.64}3p^{2.04-2.46}$	−2.29	−2.34
18	$6s^{0.58}5d^{9.06}6p^{1.54}$	$6s^{0.63}5d^{8.94}6p^{1.29}$	$3s^{1.27-1.68}3p^{2.01-2.64}$	−2.19	−1.87

i) As is shown in fig. 4(a), $E_b(n)$ of the Ir_2Si_n clusters is slightly smaller than that of pure Si_{n+2} clusters, indicating that the thermodynamic stabilities of the Si_{n+2} cluster with iridium doping go down. Similar scenarios also have been reported in the previous articles of X_2Si_n (X = Cu, Pd and Zr) clusters [29–31]. It is easily found that for Ir_2-doped Si_n clusters, the $E_b(n)$ values increase slowly with cluster size growing and three unconspicuous peaks are found at n = 5, 7, 12 and 16, implies that the higher stabilities of the Ir_2Si_5 and Ir_2Si_7 clusters.

ii) The Δ_2E and E_f values for the most stable Ir_2Si_n clusters are illustrated in fig. 4(b). Figure 4(b) shows that the two curves have a similar variation trend except for n = 2 and 8. For $\Delta_2E(n)$, four conspicuous maxima are found at n = 3, 6, 9, 11 and 16, indicating that the $Ir_2Si_{3,6,9,11,16}$ clusters are more stable than the others. For $E_f(n)$, four peaks appear at the size of 2, 6, 9, 11 and 16, signifying that Ir_2Si_2, Ir_2Si_6, Ir_2Si_9, Ir_2Si_{11} and Ir_2Si_{16} clusters have relatively strong stabilities.

iii) The E_{gap} values of the most stable Ir_2Si_n and Si_{n+2} clusters are shown in fig. 4(c). A large value of E_{gap} is an indication of the relative stabilities as the cluster wants to neither receive nor donate electrons. Comparing the E_{gap} values of Ir_2Si_n and Si_{n+2} clusters, one can see that the E_{gap} values of Ir_2Si_n are always the lowest, which signifies that the Ir atoms can reduce the stabilities of the Si_{n+2} clusters. It is worth noting that for the Ir_2Si_n clusters, the E_{gap} values decrease monotonically with cluster size growing except for n = 1, 3, 6, 9, 11, 14 and 17, which implies that the Ir_2Si, Ir_2Si_3, Ir_2Si_6, Ir_2Si_9, Ir_2Si_{11}, Ir_2Si_{14}, and Ir_2Si_{17} clusters have stabilities higher than those of other Ir_2Si_n clusters (n = 2, 4, 5, 7, 8, 10, 12, 13, 15, 16, and 18).

To study the natural bond, the electronic structure and distribution of HOMOs for the most stable Ir_2Si_n (n = 1–18) clusters are analyzed. In Si_2 cluster, the π-type bond is found between the Si-Si bonds. And yet, the π-type bond is changed to be of σ-type bond after one Ir atom is capped on the Si_2 dimer. In the Ir_2Si_n clusters, some π-type and σ-type bonds are found among these Si atoms. The Ir and Si atoms want to form σ-type bonding with an overlap between vacant in-plane p orbitals of Si atoms and valence d orbitals of Ir atoms.

3.3 Natural population analysis

To study the inside charge transfer mechanism of the Ir_2Si_n (n = 1–18) clusters deeply, the natural population analysis (NPA) and natural electron configurations (NEC) for the most stable Ir_2Si_n clusters are computed and listed in table 3. From table 3, it is clear that the atomic charges on the Ir atoms ($-0.20e$ to $-3.04e$) are negative charges, which is exactly what we expected, *i.e.* the charges in these clusters transfer from Si atoms to Ir atoms. Namely, the Ir atom acts as an electron acceptor. That may be that Ir (2.20) has higher electronegativity than that of Si (1.90) [43].

Moreover, one interesting phenomenon is that the charges for Ir atoms in the $Ir_2Si_{1,2,3,6,16}$ clusters are equal, but they are different in the $Ir_2Si_{4,5,7-15,17,18}$ clusters, which may be related to the fact that there are equal numbers of Ir-Si bonds in Ir_2Si, Ir_2Si_2, Ir_2Si_3, Ir_2Si_6 and Ir_2Si_{16} clusters; namely, the charge distribution mainly depends on the symmetry of the cluster. This result is in line with the previous NPA of Cu_2Si_n, Pd_2Si_n and Zr_2Si_n clusters [29–31]. Also, it is worth noting that the encapsulated Ir atom in Ir_2Si_{10-14} receives more charges from its surroundings than the surface-capped Ir atom does, and that the encapsulated Ir atom has relative stronger ability to interact with more Si atoms with unequivalent bond lengths. So the doped Ir atoms play a very important role in the stabilities of the Ir_2Si_n clusters. In the case of Ir_2 encapsulated silicon caged clusters, the two iridium atoms have more negative charges, which maybe caused by the cage effect. The result of NEC for Ir and Si atoms is summarized in table 2. For the Ir_2Si_n clusters, the configuration of valence electron is $5d^x6S^y6P^z$ ($8.16 \leq x \leq 9.20$, $0.50 \leq y \leq 1.71$, $0.10 \leq z \leq 2.26$) for the Ir atom and $3S^{x'}3P^{y'}(1.29 \leq x' \leq 1.80, 1.59 \leq y' \leq 2.95)$ for the Si atom. One can find that the 5d, 6s and 6p orbitals of the Ir atoms behave remarkably as core orbitals, yet the contributions of 6d, 7s and 7p are nearly zero. That is, the charges transfer from 6s orbital to 5d and 6p orbitals for Ir atom. Therefore, there is strong spd hybridization in the Ir atom. In addition, the sp hybridization in the Si atom deriving from charges transfer from 3s orbital to 3p orbital is also found. In addition, the % hybridization of different orbitals from Si and Ir atoms in the lowest-energy Ir_2Si_n ($n = 15$–18) clusters are listed in table S1.

3.4 Electrostatic potential

It is generally known that the electrostatic potential (ESP), as a very useful tool for the study of the behaviour of chemical reactions (for example, halogen bonds, molecular recognitions, and so on), plays a very important role [44,45]. Here, the ESP of lowest-energy Ir_2Si_n clusters is calculated by using Multiwfn [46]. The ESP ($V(r)$) can be given by

$$V(r) = \sum_A \frac{Z_A}{|R_A - r|} - \int \frac{\rho(r')}{|r' - r|} \mathrm{d}r'. \tag{4}$$

In formula (4), R_A and Z_A represent the position vector and the number of expressed electrons, respectively. The $\rho(r')$ is a pre-fitted electron density function of the position vector $\vec{r'}$. The symbol of $V(r)$ in any given area hinges on whether the effects of the electrons or the nuclei are dominant there. A negative (positive) value signifies that the current position is dominated by electronic (nuclear) charges. Here, the isosurface of ESP for the ground state Ir_2Si_n clusters are plotted in figs. S3–20 (in the Supplementary Material). In figs. S3–20, the dashed and solid lines correspond to the negative and positive isopotential, respectively. The real blue line corresponds to the van der Waals (vdW) surface (isosurface of electron density = 0.001 a.u.). The areas enclosed by blue lines are internal regions of the molecule and will not be considered. One can clearly see the local vdW surface around the Ir atom (dashed line), which implies that the surroundings of Ir atoms have negative potential. This is consistent with the previous results of NPA, according to which the two Ir atoms possess negative charges. At the same time, the isopotential lines close to the Si atoms always show positive potential, which means that the electron density of the region between the two adjacent Si atoms decreases.

3.5 Infrared and Raman spectra

To further investigate the stabilities of Ir_2Si_n clusters, the vibrational spectra (infrared and Raman) of Ir_2Si_6, Ir_2Si_9 and Ir_2Si_{11} clusters are calculated and illustrated in figs. 5(a) and (b). Moreover, the molecular graphs of Ir_2Si_6, Ir_2Si_9 and Ir_2Si_{11} are displayed in the Supplementary Material (fig. S21).

As can be seen from fig. 5(a), two conspicuous peaks are found in the infrared (IR) spectra of Ir_2Si_6. The strongest intense peak of IR at frequency 295.79 cm^{-1} is 37.53 km/mol, which corresponds to the antisymmetric stretching vibration of Ir7-Si6 and Ir8-Si2 bonds. The second degenerate IR intense peak appears at frequency 110.79 cm^{-1}, which comes from the breathing vibration of Ir_2Si_6 cluster. For Ir_2Si_9, two local peaks of IR spectra occur at the frequencies of 398.57 cm^{-1} and 420.40 cm^{-1}, respectively. The stretching vibration of Si7-Si3, Si10-Si5, Si7-Si6 and Si10-Si2 bonds give rise to the strongest intense IR peak, whereas the second degenerate IR peak corresponds to the stretching vibration of Ir9-Si2 and Ir9-Si3 bonds. For Ir_2Si_{11}, the maximum intense visible peak of IR at frequency 175.07 cm^{-1} is assigned to the wagging vibration of Si6-Si5 and Si4-Si9 bonds. In fig. 5(b), the Raman spectrum of the Ir_2Si_6, Ir_2Si_9 and Ir_2Si_{11} clusters are plotted. For Ir_2Si_6, there are three visible peaks. The highest Raman activity peak at frequency 409.70 cm^{-1} is 10.85 $Å^4$/amu, which corresponds to the breathing vibration of the Ir_2Si_6 cluster. The double and triply degenerate Raman frequencies at 90.65 cm^{-1} and 307.48 cm^{-1} mainly result from the antisymmetric wagging vibration of Si6-Si3 and Si4-Si2 bonds. For Ir_2Si_9, the highest Raman activity (6.80 $Å^4$/amu) at frequency 356.59 cm^{-1} comes from the antisymmetric stretching vibration of Si8-Si5 and Si8-Si6 bonds. Another

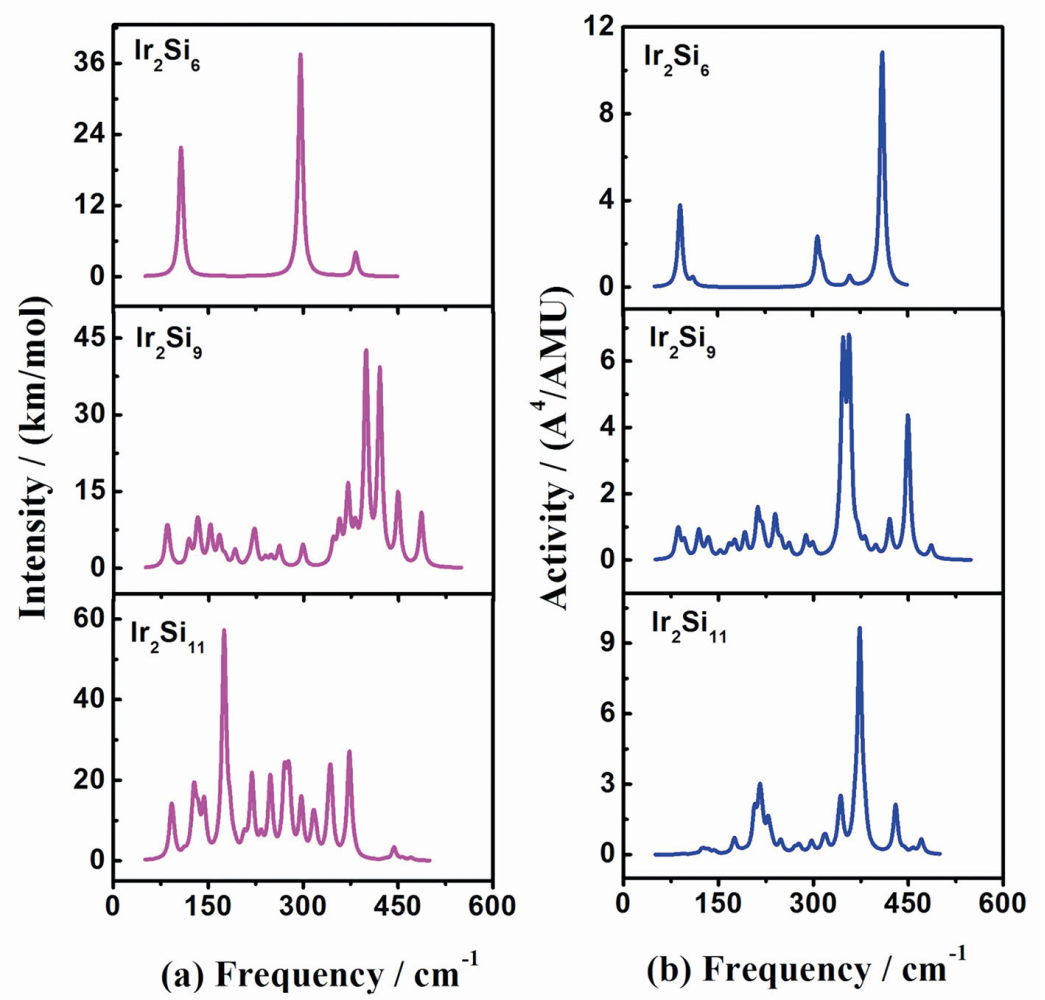

Fig. 5. The infrared intensity (a) and Raman activity (b) of Ir_2Si_6, Ir_2Si_9 and Ir_2Si_{11}.

higher peak (6.73 Å^4/amu) appears at frequency 346.77 cm^{-1}, which results from the breathing vibration of Ir11-Si3, Ir11-Si6, Si7-Si3 and Si7-Si6 bonds, as well as stretching vibration of Si10-Si2 and Si10-Si5 together. Moreover, there is a weak peak at frequency 459.33 cm^{-1} resulting from the stretching vibration of Si4. For Ir_2Si_{11}, only one obvious peak of raman spectra at 373.09 cm^{-1} is found, which comes from the stretching vibration of Si2-Si11 bond.

4 Conclusion

The structural evolution, and electronic properties of Ir_2Si_n (n = 1–18) clusters are studied in detail by using the DFT at B3LYP/GENECP level. The study results are as follows: i) The most stable structures of the Ir_2-doped Si_n (n = 1–18) clusters favor the singlet spin, with the exception of n = 1, and exhibit 3D configuration from n = 2. In addition, most of the ground state geometries of Ir_2Si_n clusters are not similar to the corresponding pure Si_{n+2} clusters. ii) The calculated results of stability indicate that Ir_2Si_6, Ir_2Si_9 and Ir_2Si_{11} clusters have enhanced stability compared with other clusters and the stability of pure Si_n clusters is reduced by the Ir atoms. iii) The NPA results show that the two Ir atoms always possess negative charges in the Ir_2Si_n clusters. So, the ESP close to the Ir atoms has negative potential.

This work is supported by the Innovation Scientists and Technicians Troop Construction Projects of Henan Province (No. C20150029), the Natural Science Foundation of Henan Province (No. 132102210048) and the Colleges and Universities Key Scientific Research Project of Henan Province (Nos. 16A140017 and 16A430023).

References

1. J.A. Alonso, Chem. Rev. **100**, 637 (2000).
2. W. Wan, X.J. Kuang, Eur. Phys. J. Plus **131**, 285 (2016).
3. R. Ferrando, J. Jellinek, R.L. Johnson, Chem. Rev. **108**, 845 (2008).
4. J.A. Alonso, *Structure and Properties of Atomic Nanoclusters* (Imperial College Press, 2012).
5. F. Calvo, *Nanoalloys: From Fundamentals to Emergent Applications* (Elsevier, 2013).
6. R. Shastri, A.K. Yadav, D. Kumar, Eur. Phys. J. Plus **132**, 313 (2017).
7. Z.J. Wu, Chem. Phys. Lett. **406**, 24 (2005).
8. B.K. Vlasta, B. Jaroslav, M. Rolan, M. Ge, Z. Giuseppe, F. Piercarlo, J. Chem. Phys. **117**, 3120 (2002).
9. L.P. Ding, X.Y. Kuang, P. Shao, M.M. Zhong, Y.F. Li, Z. Naturforsch. A **67**, 729 (2012).
10. K. Koyasu, J. Atobe, M. Akutsu, M. Mitsui, A. Nakajima, J. Phys. Chem. A **111**, 42 (2007).
11. V.T. Ngan, E. Janssens, P. Claes, J.T. Lyon, A. Fielicke, M.T. Nguyen, P. Lievens, Chem. Eur. J. **18**, 15788 (2014).
12. Y.J. Li, N.M. Tam, P. Claes, A.P. Woodham, J.T. Lyon, V.T. Ngan, M.T. Nguyen, P. Lievens, A. Fielicke, E. Janssens, J. Phys. Chem. A **118**, 8198 (2014).
13. R. Robles, S.N. Khanna, Phys. Rev. B **77**, 235441 (2008).
14. R. Roblesa, S.N. Khanna, J. Chem. Phys. **130**, 164313 (2009).
15. D. Bandyopadhyay, J. Appl. Phys. **104**, 084308 (2008).
16. T. Iwasa, A. Nakajima, J. Phys. Chem. C **116**, 14071 (2012).
17. X.X. Ji, J. Li, C. Wang, S. Zhang, C. Lu, G.Q. Li, Mol. Phys. **113**, 3567 (2015).
18. X.X. Xia, A. Hermann, X.Y. Kuang, Y.Y. Jin, C. Lu, X.D. Xing, J. Phys. Chem. C **120**, 677 (2015).
19. S. Zhang, Y. Zhang, X.Q. Yang, C. Lu, G.Q. Li, Z.W. Lu, J. Mater. Sci. **50**, 6180 (2015).
20. X. Ma, Thin Solid Films. **484**, 257 (2005).
21. A.V. Auwera-Mahieu, R. Peeters, N.S. McIntyre, J. Drowart, Trans. Faraday Soc. **66**, 809 (1970).
22. M.A. Garcia, C. Vietz, F. Ruipérez, M.D. Morse, I. Infante, J. Chem. Phys. **138**, 154306 (2013).
23. H. Hiura, T. Miyazaki, T. Kanayama, Phys. Rev. Lett. **86**, 1733 (2001).
24. J.G. Han, Chem. Phys. **286**, 181 (2003).
25. C. Pouchan, D. Bégue, D.Y. Zhang, J. Chem. Phys. **121**, 4628 (2004).
26. S. Li, R.J. Van Zee, W. Weltner Jr., K. Raghavachari, Chem. Phys. Lett. **243**, 275 (1995).
27. M. Haertelt, J.T. Lyon, P. Claes, J.D. Haeck, P. Lievens, A. Fielicke, J. Chem. Phys. **136**, 064301 (2012).
28. W. Qin, W.C. Lu, L.Z. Zhao, Q.J. Zang, C.Z. Wang, K.M. Ho, J. Phys.: Condens. Matter **21**, 455501 (2009).
29. P. Shao, X.Y. Kuang, L.P. Ding, M.M. Zhong, Z.H. Wang, Physica B **407**, 4379 (2012).
30. R.N. Zhao, J.G. Han, Y.H. Duan, Thin Solid Films **556**, 571 (2014).
31. J.H. Wu, C.X. Liu, P. Wang, S. Zhang, G. Yang, C. Lu, Z. Naturforsch. A **70**, 805 (2015).
32. J.G. Han, R.N. Zhao, Y.H. Duan, J. Phys. Chem. A **111**, 2148 (2007).
33. S. Zhang, C.G. Luo, H.Y. Li, C. Lu, G.Q. Li, Z.W. Lu, Mater. Chem. Phys. **160**, 227 (2015).
34. H.G. Xu, Z.G. Zhang, Y. Feng, W.J. Zheng, Chem. Phys. Lett. **498**, 22 (2010).
35. A.D. Becke, Phys. Rev. A **38**, 3098 (1988).
36. C. Lee, W. Yang, R.G. Parr, Phys. Rev. B **37**, 785 (1988).
37. M.J. Frisch *et al.*, *GAUSSIAN 09 Revision C.01* (Gaussian, Inc., Wallingford, CT, 2009).
38. M.A. Garcia, C. Vietz, F. Ruipérez, M.D. Morse, I. Infante, J. Chem. Phys. **138**, 154306 (2013).
39. J.L. Jules, J.R. Lombardi, J. Phys. Chem. A **107**, 1268 (2003).
40. A.R. Miedema, K.A. Gingerich, J. Phys. B **12**, 2081 (1979).
41. K.P. Huber, G. Herzberg, *Molecular Spectra and Molecular Structure IV: Constants of diatomic molecules* (Van Nostrand Reinhold, New York, 1979).
42. W.A. de Heer, W.D. Knight, M.Y. Chou, M.L. Cohen, Solid State Phys. **40**, 93 (1987).
43. G.D. Zhou, L.Y. Duan, *Structural Chemistry Basis* (Peking University Press, Beijing, 2002).
44. J.S. Murray, P. Politzer, J. Mol. Struct.: Theochem **425**, 107 (1998).
45. P. Politzer, J.S. Murray, Trends Chem. Phys. **7**, 157 (1999).
46. T. Lu, F.W. Chen, J. Mol. Graph. Model. **38**, 314 (2012).